7-1-2010

Transverse momentum dependence of J/psi polarization at midrapidity in p plus p collisions at root s=200 GeV

Andrew Adare
University of Colorado, Boulder

John C. Hill
Iowa State University, jhill@iastate.edu

Todd Kempel
Iowa State University, todd.kempel@gmail.com

John G. Lajoie
Iowa State University, lajoie@iastate.edu

Alexandre Lebedev
Iowa State University, lebedev@iastate.edu

See next page for additional authors

Transverse momentum dependence of J/psi polarization at midrapidity in p plus p collisions at root s=200 GeV

Abstract
We report the measurement of the transverse momentum dependence of inclusive J/psi polarization in p + p collisions at root s = 200 GeV performed by the PHENIX Experiment at the Relativistic Heavy Ion Collider. The J/psi polarization is studied in the helicity, Gottfried-Jackson, and Collins-Soper frames for p(T) < 5 GeV/c and vertical bar y vertical bar < 0.35. The polarization in the helicity and Gottfried-Jackson frames is consistent with zero for all transverse momenta, with a slight (1.8 sigma) trend towards longitudinal polarization for transverse momenta above 2 GeV/c. No conclusion is allowed due to the limited acceptance in the Collins-Soper frame and the uncertainties of the current data. The results are compared to observations for other collision systems and center of mass energies and to different quarkonia production models.

Disciplines
Elementary Particles and Fields and String Theory | Physics

Comments
This article is published as Adare, A., S. Afanasiev, C. Aidala, N. N. Ajitanand, Yasuyuki Akiba, H. Al-Bataineh, J. Alexander et al. "Transverse momentum dependence of J/ψ polarization at midrapidity in p+ p collisions at s= 200 GeV." *Physical Review D* 82, no. 1 (2010): 012001. DOI:10.1103/PhysRevD.82.012001. Posted with permission.

Authors
Andrew Adare, John C. Hill, Todd Kempel, John G. Lajoie, Alexandre Lebedev, Craig Ogilvie, H. Pei, Marzia Rosati, Alexey Yu. Semenov, Carla Vale, Feng Wei, et al., and PHENIX Collaboration

Transverse momentum dependence of J/ψ polarization at midrapidity in $p + p$ collisions at $\sqrt{s} = 200$ GeV

A. Adare,[11] S. Afanasiev,[25] C. Aidala,[36] N. N. Ajitanand,[53] Y. Akiba,[47,48] H. Al-Bataineh,[42] J. Alexander,[53] K. Aoki,[30,47] L. Aphecetche,[55] J. Asai,[47] E. T. Atomssa,[31] R. Averbeck,[54] T. C. Awes,[43] B. Azmoun,[6] V. Babintsev,[21] M. Bai,[5] G. Baksay,[17] L. Baksay,[17] A. Baldisseri,[14] K. N. Barish,[7] P. D. Barnes,[33] B. Bassalleck,[41] A. T. Basye,[1] S. Bathe,[7] S. Batsouli,[43] V. Baublis,[46] C. Baumann,[37] A. Bazilevsky,[6] S. Belikov,[6,*] R. Bennett,[54] A. Berdnikov,[50] Y. Berdnikov,[50] A. A. Bickley,[11] J. G. Boissevain,[33] H. Borel,[14] K. Boyle,[54] M. L. Brooks,[33] H. Buesching,[6] V. Bumazhnov,[21] G. Bunce,[6,48] S. Butsyk,[33] C. M. Camacho,[33] S. Campbell,[54] B. S. Chang,[62] W. C. Chang,[2] J.-L. Charvet,[14] S. Chernichenko,[21] C. Y. Chi,[12] M. Chiu,[22] I. J. Choi,[62] R. K. Choudhury,[4] T. Chujo,[58] P. Chung,[53] A. Churyn,[21] V. Cianciolo,[43] Z. Citron,[54] B. A. Cole,[12] Z. Conesa del Valle,[31] P. Constantin,[33] M. Csanád,[16] T. Csörgö,[27] T. Dahms,[54] S. Dairaku,[30,47] K. Das,[18] G. David,[6] A. Denisov,[21] D. d'Enterria,[31] A. Deshpande,[48,54] E. J. Desmond,[6] O. Dietzsch,[51] A. Dion,[54] M. Donadelli,[51] O. Drapier,[31] A. Drees,[54] K. A. Drees,[5] A. K. Dubey,[61] A. Durum,[21] D. Dutta,[4] V. Dzhordzhadze,[7] Y. V. Efremenko,[43] F. Ellinghaus,[11] T. Engelmore,[12] A. Enokizono,[32] H. En'yo,[47,48] S. Esumi,[58] K. O. Eyser,[7] B. Fadem,[38] D. E. Fields,[41,48] M. Finger, Jr.,[8] M. Finger,[8] F. Fleuret,[31] S. L. Fokin,[29] Z. Fraenkel,[61,†] J. E. Frantz,[54] A. Franz,[6] A. D. Frawley,[18] K. Fujiwara,[47] Y. Fukao,[30,47] T. Fusayasu,[40] I. Garishvili,[56] A. Glenn,[11] H. Gong,[54] M. Gonin,[31] J. Gosset,[14] Y. Goto,[47,48] R. Granier de Cassagnac,[31] N. Grau,[12] S. V. Greene,[59] M. Grosse Perdekamp,[22,48] T. Gunji,[10] H.-Å. Gustafsson,[35,‡] A. Hadj Henni,[55] J. S. Haggerty,[6] H. Hamagaki,[10] R. Han,[45] E. P. Hartouni,[32] K. Haruna,[20] E. Haslum,[35] R. Hayano,[10] M. Heffner,[32] T. K. Hemmick,[54] T. Hester,[7] X. He,[19] J. C. Hill,[24] M. Hohlmann,[17] W. Holzmann,[53] K. Homma,[20] B. Hong,[28] T. Horaguchi,[10,47,57] D. Hornback,[56] S. Huang,[59] T. Ichihara,[47,48] R. Ichimiya,[47] Y. Ikeda,[58] K. Imai,[30,47] J. Imrek,[15] M. Inaba,[58] D. Isenhower,[1] M. Ishihara,[47] T. Isobe,[10] M. Issah,[53] A. Isupov,[25] D. Ivanischev,[46] B. V. Jacak,[54,§] J. Jia,[12] J. Jin,[12] B. M. Johnson,[6] K. S. Joo,[39] D. Jouan,[44] F. Kajihara,[10] S. Kametani,[47] N. Kamihara,[48] J. Kamin,[54] J. H. Kang,[62] J. Kapustinsky,[33] D. Kawall,[36,48] A. V. Kazantsev,[29] T. Kempel,[24] A. Khanzadeev,[46] K. M. Kijima,[20] J. Kikuchi,[60] B. I. Kim,[28] D. H. Kim,[39] D. J. Kim,[62] E. Kim,[52] S. H. Kim,[62] E. Kinney,[11] K. Kiriluk,[11] A. Kiss,[16] E. Kistenev,[6] J. Klay,[32] C. Klein-Boesing,[37] L. Kochenda,[46] B. Komkov,[46] M. Konno,[58] J. Koster,[22] A. Kozlov,[61] A. Král,[13] A. Kravitz,[12] G. J. Kunde,[33] K. Kurita,[49,47] M. Kurosawa,[47] M. J. Kweon,[28] Y. Kwon,[56] G. S. Kyle,[42] R. Lacey,[53] Y. S. Lai,[12] J. G. Lajoie,[24] D. Layton,[22] A. Lebedev,[24] D. M. Lee,[33] K. B. Lee,[28] T. Lee,[52] M. J. Leitch,[33] M. A. L. Leite,[51] B. Lenzi,[51] P. Liebing,[48] T. Liška,[13] A. Litvinenko,[25] H. Liu,[42] M. X. Liu,[33] X. Li,[9] B. Love,[59] D. Lynch,[6] C. F. Maguire,[59] Y. I. Makdisi,[5] A. Malakhov,[25] M. D. Malik,[41] V. I. Manko,[29] E. Mannel,[12] Y. Mao,[45,47] L. Mašek,[8,23] H. Masui,[58] F. Matathias,[12] M. McCumber,[54] P. L. McGaughey,[33] N. Means,[54] B. Meredith,[22] Y. Miake,[58] P. Mikeš,[23] K. Miki,[58] A. Milov,[6] M. Mishra,[3] J. T. Mitchell,[6] A. K. Mohanty,[4] Y. Morino,[10] A. Morreale,[7] D. P. Morrison,[6] T. V. Moukhanova,[29] D. Mukhopadhyay,[59] J. Murata,[49,47] S. Nagamiya,[26] J. L. Nagle,[11] M. Naglis,[61] M. I. Nagy,[16] I. Nakagawa,[47,48] Y. Nakamiya,[20] T. Nakamura,[20] K. Nakano,[47,57] J. Newby,[32] M. Nguyen,[54] T. Niita,[58] R. Nouicer,[6] A. S. Nyanin,[29] E. O'Brien,[6] S. X. Oda,[10] C. A. Ogilvie,[24] H. Okada,[30,47] K. Okada,[48] M. Oka,[58] Y. Onuki,[47] A. Oskarsson,[35] M. Ouchida,[20] K. Ozawa,[10] R. Pak,[6] A. P. T. Palounek,[33] V. Pantuev,[54] V. Papavassiliou,[42] J. Park,[52] W. J. Park,[28] S. F. Pate,[42] H. Pei,[24] J.-C. Peng,[22] H. Pereira,[14] V. Peresedov,[25] D. Yu. Peressounko,[29] C. Pinkenburg,[6] M. L. Purschke,[6] A. K. Purwar,[33] H. Qu,[19] J. Rak,[41] A. Rakotozafindrabe,[31] I. Ravinovich,[61] K. F. Read,[43,56] S. Rembeczki,[17] K. Reygers,[37] V. Riabov,[46] Y. Riabov,[46] D. Roach,[59] G. Roche,[34] S. D. Rolnick,[7] M. Rosati,[24] S. S. E. Rosendahl,[35] P. Rosnet,[34] P. Rukoyatkin,[25] P. Ružička,[23] V. L. Rykov,[47] B. Sahlmueller,[37] N. Saito,[30,47,48] T. Sakaguchi,[6] S. Sakai,[58] K. Sakashita,[47,57] V. Samsonov,[46] T. Sato,[58] S. Sawada,[26] K. Sedgwick,[7] J. Seele,[11] R. Seidl,[22] A. Yu. Semenov,[24] V. Semenov,[21] R. Seto,[7] D. Sharma,[61] I. Shein,[21] T.-A. Shibata,[47,57] K. Shigaki,[20] M. Shimomura,[58] K. Shoji,[30,47] P. Shukla,[4] A. Sickles,[6] C. L. Silva,[51] D. Silvermyr,[43] C. Silvestre,[14] K. S. Sim,[28] B. K. Singh,[3] C. P. Singh,[3] V. Singh,[3] M. Slunečka,[8] A. Soldatov,[21] R. A. Soltz,[32] W. E. Sondheim,[33] S. P. Sorensen,[56] I. V. Sourikova,[6] F. Staley,[14] P. W. Stankus,[43] E. Stenlund,[35] M. Stepanov,[42] A. Ster,[27] S. P. Stoll,[6] T. Sugitate,[20] C. Suire,[44] A. Sukhanov,[6] J. Sziklai,[27] E. M. Takagui,[51] A. Taketani,[47,48] R. Tanabe,[58] Y. Tanaka,[40] K. Tanida,[47,48] M. J. Tannenbaum,[6] A. Taranenko,[53] P. Tarján,[15] H. Themann,[54] T. L. Thomas,[41] M. Togawa,[30,47] A. Toia,[54] L. Tomášek,[23] Y. Tomita,[58] H. Torii,[20,47] R. S. Towell,[1] V-N. Tram,[31] I. Tserruya,[61] Y. Tsuchimoto,[20] C. Vale,[24] H. Valle,[59] H. W. van Hecke,[33] A. Veicht,[22] J. Velkovska,[59] R. Vertesi,[15] A. A. Vinogradov,[29] M. Virius,[13] V. Vrba,[23] E. Vznuzdaev,[46] X. R. Wang,[42] Y. Watanabe,[47,48] F. Wei,[24] J. Wessels,[37] S. N. White,[6] D. Winter,[12] C. L. Woody,[6] M. Wysocki,[11] W. Xie,[48] Y. L. Yamaguchi,[60] K. Yamaura,[20] R. Yang,[22] A. Yanovich,[21] J. Ying,[19] S. Yokkaichi,[47,48] G. R. Young,[43] I. Younus,[41] I. E. Yushmanov,[29] W. A. Zajc,[12] O. Zaudtke,[37] C. Zhang,[43] S. Zhou,[9] and L. Zolin[25]

(PHENIX Collaboration)

[1]*Abilene Christian University, Abilene, Texas 79699, USA*
[2]*Institute of Physics, Academia Sinica, Taipei 11529, Taiwan*
[3]*Department of Physics, Banaras Hindu University, Varanasi 221005, India*
[4]*Bhabha Atomic Research Centre, Bombay 400 085, India*
[5]*Collider-Accelerator Department, Brookhaven National Laboratory, Upton, New York 11973-5000, USA*
[6]*Physics Department, Brookhaven National Laboratory, Upton, New York 11973-5000, USA*
[7]*University of California-Riverside, Riverside, California 92521, USA*
[8]*Charles University, Ovocný trh 5, Praha 1, 116 36, Prague, Czech Republic*
[9]*China Institute of Atomic Energy (CIAE), Beijing, People's Republic of China*
[10]*Center for Nuclear Study, Graduate School of Science, University of Tokyo, 7-3-1 Hongo, Bunkyo, Tokyo 113-0033, Japan*
[11]*University of Colorado, Boulder, Colorado 80309, USA*
[12]*Columbia University, New York, New York 10027, and Nevis Laboratories, Irvington, New York 10533, USA*
[13]*Czech Technical University, Zikova 4, 166 36 Prague 6, Czech Republic*
[14]*Dapnia, CEA Saclay, F-91191, Gif-sur-Yvette, France*
[15]*Debrecen University, H-4010 Debrecen, Egyetem tér 1, Hungary*
[16]*ELTE, Eötvös Loránd University, H-1117 Budapest, Pázmány P. s. 1/A, Hungary*
[17]*Florida Institute of Technology, Melbourne, Florida 32901, USA*
[18]*Florida State University, Tallahassee, Florida 32306, USA*
[19]*Georgia State University, Atlanta, Georgia 30303, USA*
[20]*Hiroshima University, Kagamiyama, Higashi-Hiroshima 739-8526, Japan*
[21]*IHEP Protvino, State Research Center of Russian Federation, Institute for High Energy Physics, Protvino, 142281, Russia*
[22]*University of Illinois at Urbana-Champaign, Urbana, Illinois 61801, USA*
[23]*Institute of Physics, Academy of Sciences of the Czech Republic, Na Slovance 2, 182 21 Prague 8, Czech Republic*
[24]*Iowa State University, Ames, Iowa 50011, USA*
[25]*Joint Institute for Nuclear Research, 141980 Dubna, Moscow Region, Russia*
[26]*KEK, High Energy Accelerator Research Organization, Tsukuba, Ibaraki 305-0801, Japan*
[27]*KFKI Research Institute for Particle and Nuclear Physics of the Hungarian Academy of Sciences (MTA KFKI RMKI), H-1525 Budapest 114, P.O. Box 49, Budapest, Hungary*
[28]*Korea University, Seoul 136-701, Korea*
[29]*Russian Research Center Kurchatov Institute, Moscow, Russia*
[30]*Kyoto University, Kyoto 606-8502, Japan*
[31]*Laboratoire Leprince-Ringuet, École Polytechnique, CNRS-IN2P3, Route de Saclay, F-91128, Palaiseau, France*
[32]*Lawrence Livermore National Laboratory, Livermore, California 94550, USA*
[33]*Los Alamos National Laboratory, Los Alamos, New Mexico 87545, USA*
[34]*LPC, Université Blaise Pascal, CNRS-IN2P3, Clermont-Fd, 63177 Aubiere Cedex, France*
[35]*Department of Physics, Lund University, Box 118, SE-221 00 Lund, Sweden*
[36]*Department of Physics, University of Massachusetts, Amherst, Massachusetts 01003-9337, USA*
[37]*Institut für Kernphysik, University of Muenster, D-48149 Muenster, Germany*
[38]*Muhlenberg College, Allentown, Pennsylvania 18104-5586, USA*
[39]*Myongji University, Yongin, Kyonggido 449-728, Korea*
[40]*Nagasaki Institute of Applied Science, Nagasaki-shi, Nagasaki 851-0193, Japan*
[41]*University of New Mexico, Albuquerque, New Mexico 87131, USA*
[42]*New Mexico State University, Las Cruces, New Mexico 88003, USA*
[43]*Oak Ridge National Laboratory, Oak Ridge, Tennessee 37831, USA*
[44]*IPN-Orsay, Universite Paris Sud, CNRS-IN2P3, BP1, F-91406, Orsay, France*
[45]*Peking University, Beijing, People's Republic of China*
[46]*PNPI, Petersburg Nuclear Physics Institute, Gatchina, Leningrad Region, 188300, Russia*
[47]*RIKEN Nishina Center for Accelerator-Based Science, Wako, Saitama 351-0198, Japan*
[48]*RIKEN BNL Research Center, Brookhaven National Laboratory, Upton, New York 11973-5000, USA*
[49]*Physics Department, Rikkyo University, 3-34-1 Nishi-Ikebukuro, Toshima, Tokyo 171-8501, Japan*
[50]*Saint Petersburg State Polytechnic University, St. Petersburg, Russia*
[51]*Universidade de São Paulo, Instituto de Física, Caixa Postal 66318, São Paulo CEP05315-970, Brazil*
[52]*Seoul National University, Seoul 151-742, Korea*
[53]*Chemistry Department, Stony Brook University, Stony Brook, SUNY, New York 11794-3400, USA*
[54]*Department of Physics and Astronomy, Stony Brook University, SUNY, Stony Brook, New York 11794, USA*
[55]*SUBATECH (Ecole des Mines de Nantes, CNRS-IN2P3, Université de Nantes) BP 20722—44307, Nantes, France*
[56]*University of Tennessee, Knoxville, Tennessee 37996, USA*

[57]*Department of Physics, Tokyo Institute of Technology, Oh-okayama, Meguro, Tokyo 152-8551, Japan*
[58]*Institute of Physics, University of Tsukuba, Tsukuba, Ibaraki 305, Japan*
[59]*Vanderbilt University, Nashville, Tennessee 37235, USA*
[60]*Waseda University, Advanced Research Institute for Science and Engineering, 17 Kikui-cho, Shinjuku-ku, Tokyo 162-0044, Japan*
[61]*Weizmann Institute, Rehovot 76100, Israel*
[62]*Yonsei University, IPAP, Seoul 120-749, Korea*
(Received 28 April 2010; published 7 July 2010)

We report the measurement of the transverse momentum dependence of inclusive J/ψ polarization in $p + p$ collisions at $\sqrt{s} = 200$ GeV performed by the PHENIX Experiment at the Relativistic Heavy Ion Collider. The J/ψ polarization is studied in the helicity, Gottfried-Jackson, and Collins-Soper frames for $p_T < 5$ GeV/c and $|y| < 0.35$. The polarization in the helicity and Gottfried-Jackson frames is consistent with zero for all transverse momenta, with a slight (1.8 sigma) trend towards longitudinal polarization for transverse momenta above 2 GeV/c. No conclusion is allowed due to the limited acceptance in the Collins-Soper frame and the uncertainties of the current data. The results are compared to observations for other collision systems and center of mass energies and to different quarkonia production models.

DOI: 10.1103/PhysRevD.82.012001 PACS numbers: 25.75.Dw

I. INTRODUCTION

Quarkonia production in high-energy hadronic collisions is an essential tool for investigating QCD. The $Q\bar{Q}$ pair is produced in a hard scattering involving gluons, which is followed by a hadronization process that forms the bound state. These formation and hadronization steps are the subject of many studies. Initial tests of quarkonia production models using J/ψ cross sections measurements are still inconclusive [1], suggesting that other observables would be useful to challenge the different production models. For example, a key piece of information to help pin down the mechanism of heavy quarkonia ($c\bar{c}$ and $b\bar{b}$) production and the bound state formation is the angular distribution of its decay leptons.

The angular distribution of spin-$\frac{1}{2}$ lepton decay from quarkonium (spin 1) is derived from density matrix elements of the production amplitude and parity conservation rules [2–4]. The angular distribution integrated over the azimuthal angle is given by

$$\frac{d\sigma}{d\cos\theta^*} = A(1 + \lambda\cos^2\theta^*), \tag{1}$$

where A is a normalization factor and θ^* is the angle between the momentum vector of one lepton in the polarization quarkonium rest frame and the longitudinal direction ($\hat{z}$ coordinate) of a selected polarization vector (frame). The polarization parameter λ is related to the diagonal elements of the density matrix of the production amplitude and contains both the longitudinal (σ_L) and transverse (σ_T) components of the quarkonium cross section

$$\lambda = \frac{\sigma_T - 2\sigma_L}{\sigma_T + 2\sigma_L}. \tag{2}$$

The quarkonium polarization is longitudinal (transverse) in a given frame if λ is negative (positive).

The most common polarization frame used in analyses performed at collider experiments is where $\hat{z}$ is the quarkonium momentum. Polarization measured in this manner is referred to as being in the helicity frame (HX) [2]. In fixed target experiments the most frequently used polarization frame has $\hat{z}$ as one of the colliding hadrons momentum in the quarkonium rest frame, namely, the Gottfried-Jackson frame (GJ) [3]. Another polarization frame, used primarily for the studies of Drell-Yan production, is the Collins-Soper frame (CS) [4] that defines $\hat{z}$ as the bisector between the directions of the first colliding parton and of the opposite of the second colliding parton in the dilepton rest frame. A diagram representing the three polarization frames is shown in Fig. 1. The amplitude and the sign of λ depend on the frame used in the measurement. The natural polarization axis for the production process can be defined as that where the lepton decay azimuthal angle distribution is symmetric and λ is maximum [5]. In such a frame, the density matrix of the production amplitude is diagonal.

Several quarkonium production models have been proposed to describe the perturbative terms which are relevant for $Q\bar{Q}$ production, while other models include nonpertur-

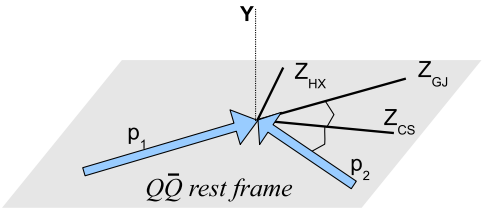

FIG. 1 (color online). Definition of the polarization frames: HX, GJ, and CS frames.

*Deceased
†Deceased
‡Deceased
§PHENIX spokesperson: jacak@skipper.physics.sunysb.edu

bative terms related to the formation of the bound state. The various models predict different polarizations and are described below.

In the color evaporation model [6], quarkonia production is assumed to be a fixed fraction of the perturbative QCD cross section for invariant masses between twice the mass of the heavy quark (c or b) and twice the mass of the open heavy quark meson (D or B). This model has reasonable agreement with most of the measured quarkonia cross sections but no predictive power for the polarization [7]. Nevertheless, according to [8], multiple soft gluon exchanges destroy the polarization of the heavy quark pair.

The earliest color singlet model (CSM) was a calculation of the leading order $gg \rightarrow S$-wave charmonium $+g$ process where the relative momentum of the $Q\bar{Q}$ pair with respect to the quark mass m_Q is neglected and the pair is produced on shell [9–11]. The $Q\bar{Q}$ binding is calculated from potential model wave functions. J/ψ yield measurements reported by CDF [12] and PHENIX [1] are largely underestimated by this model. The J/ψ polarization predicted by LO CSM is transverse in the HX frame [13]. Subsequent calculations also included next-to-leading order terms [14–16], next-to-next-to-leading order terms [17,18], and an s-channel cut contribution that allows off-shell $c\bar{c}$ quarks to end up in the bound state [19]. These calculations show large changes in the yield and polarization relative to the earlier calculations. The new calculations of the J/ψ yield is closer to what is observed in PHENIX and CDF for $p_T < 10$ GeV/c. The J/ψ polarization is predominantly longitudinal in the HX frame according to these new calculations.

Nonrelativistic QCD effective theory [20] makes use of short distance (m_Q) and nonrelativistic ($m_Q v^2$) terms, where v is the typical quark velocity in the quarkonium rest frame. A typical v for charm (bottom) is $0.3c$ ($0.1c$). The S-wave charmonium is described as a series of intermediate color singlet$^{(1)}$ or color octet$^{(8)}$ state contributions

$$|\psi_Q\rangle = \mathcal{O}(1)|^3S_1^{(1)}\rangle + \mathcal{O}(v)|^3P_J^{(8)}g\rangle + \mathcal{O}(v^2)|^3S_1^{(8)}gg\rangle + \mathcal{O}(v^2)|^3S_0^{(8)}g\rangle + \cdots, \quad (3)$$

where the spectroscopic notation $^{2S+1}L_J$ is used. The nonperturbative operators $\mathcal{O}(v)$ are parametrized using experimental results. Since the singlet state has a small contribution to the yield, this model is also referred as the color octet model (COM). Using constraints from the CDF cross section J/ψ data, reasonable agreement is obtained with PHENIX yield results assuming J/ψ production is dominated by gluon fusion in the $1S_0^{(8)}$ and $3P_0^{(8)}$ intermediate states for $p_T < 5$ GeV/c [13,21]. Calculations performed in [22] estimated $\lambda(^1S_0^{(8)}) = 0$ and $\lambda(^3P_0^{(8)}) = -0.05$ indicating a very small longitudinal polarization from direct J/ψ in this p_T range. Numerical estimations [23,24] and subsequent next-to-leading order corrections [25] supports that the polarization for $p_T \gg M_{J/\psi}$, where production from gluon fragmentation is supposed to be important, is predominantly transverse in the HX frame.

The J/ψ polarization in hadronic collisions was studied in fixed target experiments at $\sqrt{s} \leq 39$ GeV [26–33]. These experiments predominantly covered $|x_F| > 0$ and $p_T < 5$ GeV/c. In [5] it was noted that J/ψ polarization measured in the CS frame by HERA-B [31] and by E866/NuSea [33] smoothly changes from longitudinal to transverse with the total momentum. The polarization observed in CDF at $\sqrt{s} = 1.96$ TeV in midrapidity for $p_T > 5$ GeV/c showed a small longitudinal polarization in the HX frame [34]. This result contradicts the first LO CSM and COM expectations.

Complementary J/ψ polarization measurements in $p + p$ collisions at $\sqrt{s} = 200$ GeV can help elucidate the production mechanism. Moreover, it is expected that the polarization of J/ψ is modified in the presence of nuclear matter effects in $d + \mathrm{Au}$ collisions and hot and dense matter in Au + Au collisions [35]. Thus, future measurements of J/ψ polarization in $d + \mathrm{Au}$ and Au + Au at the Relativistic Heavy Ion Collider (RHIC) demands a good reference from $p + p$ collisions.

This paper reports the transverse momentum dependence of the J/ψ polarization for $|y| < 0.35$ in the HX, GJ, and CS reference frames. The study was performed in the dielectron decay channel for $p_T < 5$ GeV/c. The experimental apparatus used to measure electron decays from J/ψ mesons is detailed in Sec. II. The procedure followed to obtain the $\cos\theta^*$ distributions, the corresponding polarization parameters and their uncertainties are explained in Sec. III. The results, comparison with measurements at other facilities and interpretation in the context of current theoretical models are presented in Sec. IV.

II. EXPERIMENTAL APPARATUS AND J/ψ IDENTIFICATION

This analysis was performed with data collected in $p + p$ collisions at $\sqrt{s} = 200$ GeV during the 2006 RHIC Run with the PHENIX central arm detectors [36]. The geometrical coverage for single electrons corresponds to pseudorapidity $|\eta| < 0.35$. Each one of the roughly back-to-back two arms covers $\Delta\phi = \pi/2$.

Data were recorded using a minimum-bias trigger that required at least one hit in each of the two beam-beam counters located at $3.0 < |\eta| < 3.9$ and scanning approximately 50% of the $p + p$ cross section. A dedicated trigger (EMCal RICH Trigger—ERT) was also used to select events with at least one electron candidate. The ERT required a minimum energy in any 2×2 group of the Electromagnetic Calorimeter (EMCal) towers[1] and associated hits in the ring imaging Čerenkov detector (RICH) in coincidence with the minimum-bias trigger condition. The

[1]Corresponding to $\Delta\eta \times \Delta\phi = 0.02 \times 0.02$ rad

EMCal energy threshold was set to 0.4 GeV and 0.6 GeV for two different periods during the data taking run.

Collisions within ± 30 cm of the center of the detector along the beam direction were used in this analysis. After data quality selection, the number of collisions sampled was 143×10^9 beam-beam counters triggers, corresponding to an integrated luminosity of $\int \mathcal{L} = (6.2 \pm 0.6)\ \mathrm{pb}^{-1}$.

Electron candidates were selected from tracks reconstructed in the drift chamber and in the pad chamber with momentum larger than 0.5 GeV/c. Electron identification was achieved by requiring the tracks to be associated with at least one fired phototube within a ring radius 3.4 cm $< R_{\mathrm{ring}} <$ 8.4 cm centered on the projected track position in the RICH. In addition, the presence of a matching energy cluster in the EMCal was required within four sigma in both the position and expected energy/momentum ratio. Since the hadronic background in the J/ψ mass region is small in $p + p$ collisions, only loose electron identification criteria were used.

Dielectron pairs from J/ψ decays were counted in the invariant mass range $\in [2.9, 3.2]$ GeV/c^2. The combinatorial background was estimated using like-sign (e^+e^+ and e^-e^-) pairs. Since we evaluated the ERT efficiency using J/ψ simulation, we required that the ERT segment was fired by one of the J/ψ decayed electrons. Hence, only pairs with at least one electron matching geometrically the position of an actual ERT trigger in the event were accepted. The dielectron mass distribution in the J/ψ mass region is shown in Fig. 2. The signal/(combinatorial background) ratio was 28. After combinatorial background subtraction, we counted $2442 \pm 51 e^+e^-$ pairs with $p_T <$ 5 GeV/c in the selected J/ψ mass range. These counts include a residual continuum background, which consists mainly of correlated open heavy quark decays to electrons. This background was found to be less than 10%.

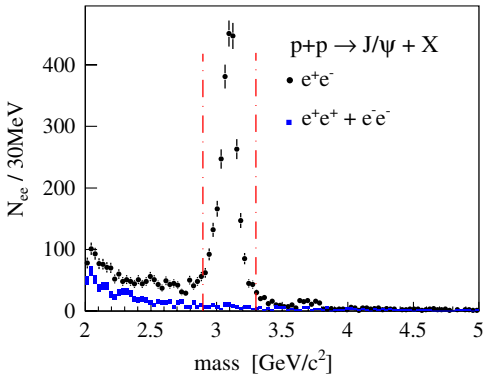

FIG. 2 (color online). Invariant mass of dielectrons in the J/ψ mass range. Dashed lines represents the mass range used in the polarization analysis.

III. ANALYSIS PROCEDURE

The angular dependence of the detector response for electrons from J/ψ decays was estimated using a full GEANT3 [37]-based detector simulation. Dead channels or malfunctioning regions were removed from the detector simulation and from the real data analysis. The experimental acceptance was checked by simulating single electrons with collision z vertex and p_T distributions weighted to reproduce observed distributions of electron candidates from real data. The raw distributions of these electrons were compared to those from simulation, after arbitrary normalization, for different azimuthal sectors (Fig. 3). Statistically significant differences in the shapes of the two distributions were attributed to conversions $\gamma \rightarrow e^+e^-$ in the detector support structure at large z which were not included in the simulation. These differences were accounted for in the systematic uncertainty listed in Table I.

The detector response to electrons in the simulation was tuned to match the data. A clean sample of electrons in the data was obtained by selecting electrons from Dalitz decays and photon conversions in the beam pipe which were identified by their very low invariant mass [38]. Figure 4 shows the comparison between the momentum dependent electron identification efficiency ($\varepsilon_{\mathrm{eID}}$) for single electrons from fully reconstructed Dalitz and photon conversion

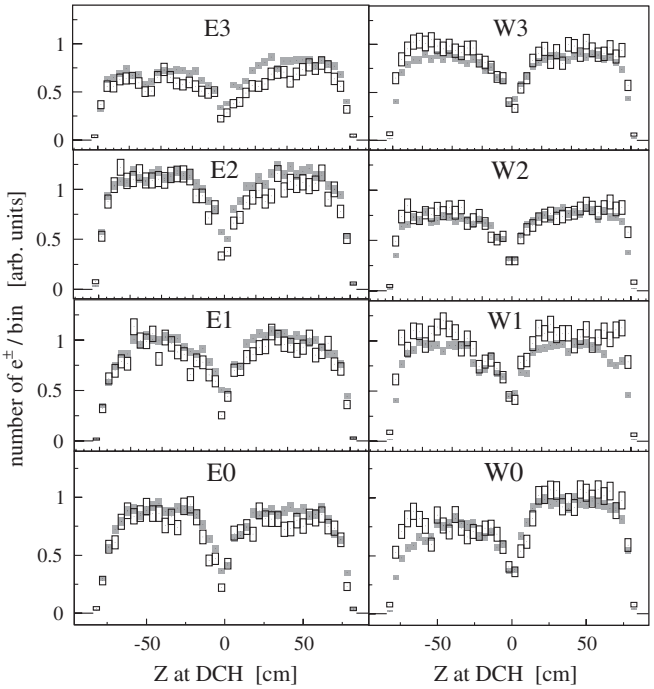

FIG. 3. Distribution of single electrons versus the Z coordinate of the track in the drift chamber for real (open boxes) and simulated (closed boxes) data for different sectors (0 is the bottom and 3 is the top ones) in the east (left) and west (right) detector arms. The box-height for each point corresponds to its statistical uncertainty.

TABLE I. Systematic uncertainties in the p_T dependent polarization measurement in the helicity and Gottfried-Jackson (in parentheses) frames.

Description	[0, 1] GeV/c	[1, 2] GeV/c	[2, 5] GeV/c	[0, 5] GeV/c
Acceptance	0.006 (0.036)	0.006 (0.012)	0.006 (0.008)	0.006 (0.024)
Polarization bias in acceptance	0.022 (0.047)	0.0011 (0.005)	0.008 (0.031)	0.012 (0.032)
Continuum fraction	$^{+0.033}_{-0.021}$ ($^{+0.091}_{-0.014}$)	$^{+0.023}_{-0.027}$ ($^{+0.032}_{-0.062}$)	$^{+0.014}_{-0.039}$ ($^{+0.023}_{-0.070}$)	$^{+0.019}_{-0.026}$ ($^{+0.032}_{-0.058}$)
Input p_T in simulation	0.034 (0.062)	0.005 (0.049)	0.024 (0.028)	0.034 (0.054)
Input y, Z vertex in simulation	0.000 (0.007)	0.000 (0.007)	0.000 (0.007)	0.000 (0.007)
Run-by-run fluctuations	0.019 (0.123)	0.016 (0.035)	0.016 (0.020)	0.017 (0.050)
ERT efficiency	0.017 (0.110)	0.015 (0.051)	0.018 (0.024)	0.015 (0.043)
TOTAL	$^{+0.06}_{-0.05}$ ($^{+0.21}_{-0.19}$)	$^{+0.03}_{-0.04}$ ($^{+0.09}_{-0.10}$)	0.04($^{+0.06}_{-0.09}$)	0.05($^{+0.09}_{-0.11}$)

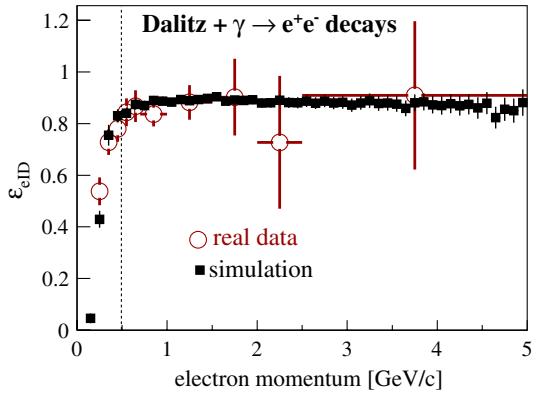

FIG. 4 (color online). Single electron identification efficiency estimated using full reconstructed Dalitz decays from real data (open circles) and simulation (full squares). Dotted line represents the minimum p_T for the electron used to reconstruct J/ψ decays.

decays in minimum-bias data and simulation. Good agreement above 0.5 GeV/c was achieved within the statistical uncertainties.

The p_T dependence of the ERT efficiency was estimated for each one of the 8 EMCal sectors by taking the fraction of minimum-bias single electron candidates that fired the ERT. These efficiencies were used in the ERT simulation. Changes in the trigger thresholds and channel masks in the ERT during the run period were used in the simulation in order to reproduce realistic run conditions.

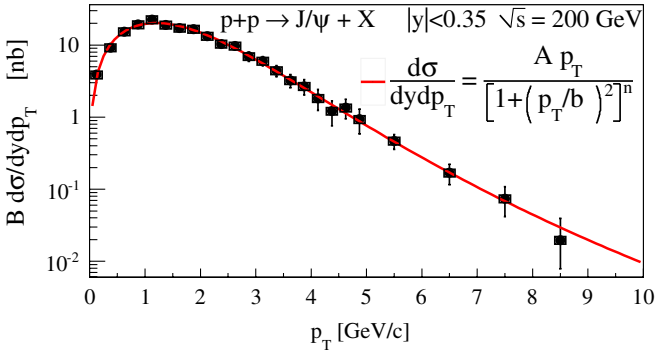

FIG. 5 (color online). Fit to J/ψ yield times dielectron branching ratio (B) after detector acceptance and efficiency corrections for the real data with $A = 28.7 \pm 1.0$ nb/GeV/c, $b = 3.41 \pm 0.21$ GeV/c, and $n = 4.6 \pm 0.4$.

The tuned detector simulation was used to reproduce the measurement of J/ψ dielectron pairs and to match their momentum, rapidity, and vertex distributions. The kinematics of the simulated J/ψ were estimated in four steps:

(1) Unpolarized $J/\psi e^+e^-$ pairs were generated with uniform distributions in rapidity ($|y| < 0.5$), p_T($p_T < 7\frac{\text{GeV}}{c}$), azimuthal angle ($-\pi < \phi < \pi$), and collision vertex along the beam axis Z($|Z_{\text{vertex}}| < 40$ cm).

(2) The $J/\psi\, p_T$ distribution obtained after applying the efficiency and acceptance corrections agrees with the previous result [1]. A Kaplan function $\frac{d\sigma}{dydp_T} = \frac{Ap_T}{[1+(p_T/b)^2]^n}$ was fit to the p_T distribution (Fig. 5), and a Gaussian function was fit to the rapidity dependence of the J/ψ yield reported in [1] and to the collision Z vertex distribution.

(3) The fitted p_T, rapidity and collision vertex functions were then used to reweight the simulated J/ψ events. The top half of each plot in Figs. 6 and 7 shows the $\cos\theta^*$ distributions in the HX, GJ, and CS frames of e^+e^- pairs in the J/ψ mass range obtained in J/ψ simulation and real data[2] after combinatorial background subtraction. The simulated and real data distributions are functions of the detector acceptance and efficiency and the original $dN_{e^+e^-}/d\cos\theta^*$ in the J/ψ mass range. The bottom panels show the ratio between the real data and simulated $\lambda = 0$ distributions, corresponding to the acceptance corrected $\cos\theta^*$ distributions.
Equation (1) was fitted to these acceptance corrected $\cos\theta^*$ distributions with no constraints on the parameters. Solid lines are the most likely fits and

[2]The $\cos\theta^*$ resolution estimated in the simulation was 0.08 in the HX, 0.025 in the GJ, and 0.007 in the CS frames. These resolutions are much smaller than the bin width of the $\cos\theta^*$ distributions used in the polarization analysis.

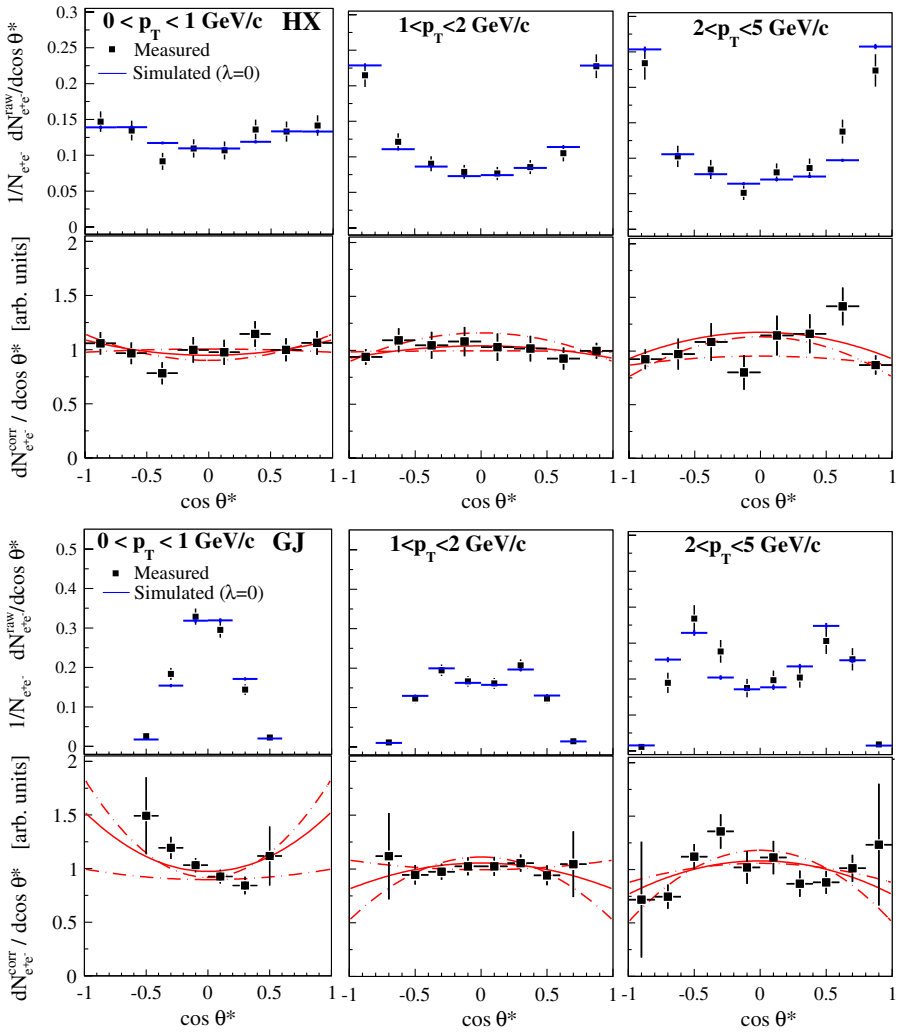

FIG. 6 (color online). Each of the six plots shows (upper half) $\cos\theta^*$ distributions of positrons decayed from (solid points) measured and (horizontal bars) simulated J/ψ mesons and (lower half) acceptance corrected distributions obtained from the ratio between real and simulated J/ψ distributions. Fits to Eq. (1) are represented as solid lines. Dashed lines correspond to one standard variation of the parameters in the fit. The top three plots are for the HX frame and the bottom three are for the GJ frame, where the smaller $\cos\theta^*$ range causes larger uncertainties of the fits.

dashed lines represent 68% confidence level interval. In the CS frame, the fit returned a polarization which was out of the physical limits ($\lambda \in [-1, 1]$). This was a result of the small acceptance for the $\cos\theta^*$ distribution in the PHENIX central arms for this frame, leading to a large statistical uncertainty on its polarization measurements. Thus, the CS frame is no longer considered in this article.

(4) Any asymmetry in the electron decay distribution, i.e. $\lambda \neq 0$, can change the detector acceptance. Hence, the fourth and final step of the simulation was to apply a weight in $\cos\theta^*$ to the simulated J/ψ by using the λ obtained in the third step. When using this realistic angular distribution for the p_T dependent acceptance, and the corresponding uncertainties, we obtained a variation in the yield up to $\pm 8\%$ for $p_T < 5$ GeV/c that corresponds to changes in polarization results no larger than 0.02 in the HX frame and 0.05 in the GJ frame. These variations were accounted for in the systematic uncertainties.

We also estimated the contribution to the J/ψ polarization from the continuum background by measuring λ in the dielectron mass range $[1.7, 2.3]$ GeV/c^2. The acceptance and efficiency corrections were performed using simulated $D\bar{D} \rightarrow$ decays, the dominant source of e^+e^- pairs in $[1.7, 2.3]$ GeV/c^2, according to the analysis in [39]. The polarization in this mass range is consistent with zero, with values between ± 0.3 in the HX and ± 0.9 in the GJ frame. The 10% continuum contribution can change the measured polarization in the J/ψ mass range by at most $\lambda(\text{HX frame})^{+0.05}_{-0.02}$ and $\lambda(\text{GJ frame})^{+0.17}_{-0.14}$ and was included in the systematic uncertainties.

The λ measurement is also sensitive to differences between acceptance in simulated and in real data, run-by-run

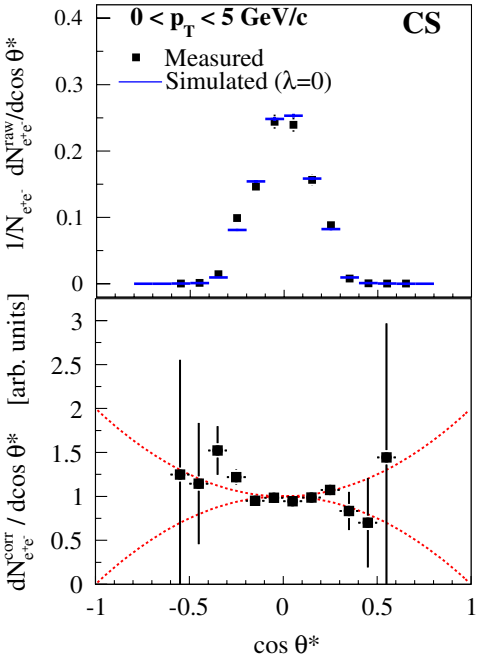

FIG. 7 (color online). (top) Same as in As in Fig. 6, but now for the Collins-Soper frame. Dotted lines on bottom panel correspond to Eq. (1) for $\lambda = \pm 1$.

condition variations, uncertainties in rapidity, Z vertex, and transverse momentum shape inputs to the simulation, as well as the ERT efficiency p_T shape. These uncertainties were introduced as variations in the efficiency and weighting parameters for different detector sectors in the simulation. Resulting variations in λ were accounted for as systematic uncertainties and are listed in Table I. The systematic uncertainties are correlated between different p_T ranges. The total systematic uncertainty is taken to be the quadratic sum of these components, assuming they are uncorrelated. Additional checks included the variation of the minimum momentum requirement of the single electrons and the rejection of tracks going to the edges of the detector. These variations returned only statistical fluctuations in the polarization results.

IV. RESULTS

Figure 8 shows the transverse momentum dependence of the J/ψ polarization in the HX and GJ frames. The uncertainties of the fit are larger in the GJ frame given the smaller $\cos\theta^*$ range compared to the HX frame. The numerical values are listed in Table II. Also shown are the current available theoretical models: COM [13] and the s-channel cut CSM [19] calculated for the HX frame. There are no theoretical predictions for the GJ frame.

The measurements presented here are for inclusive J/ψ. Feed-down from χ_c and ψ' may also contribute to the observed polarization and are not separated out. The world average result for the feed-down contribution to the J/ψ yield is $33 \pm 5\%$ [40]. The polarization of the indirect J/ψ should be smeared during the decay process. If the J/ψ

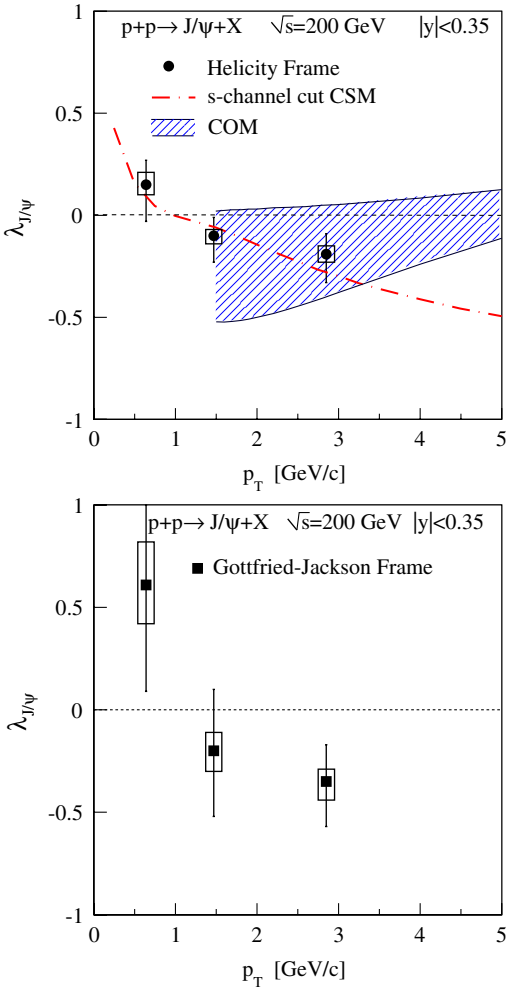

FIG. 8 (color online). J/ψ polarization parameter ($\lambda_{J/\psi}$) versus transverse momentum (p_T). Boxes are correlated systematic uncertainties. (upper) Helicity frame data is compared with COM [13] and s-channel CSM [19] calculated in the same polarization frame, but there is no prediction for the color evaporation model. (lower) There are no theoretical predictions for the Gottfried-Jackson frame.

from feed-down sources are unpolarized, the direct J/ψ may have a larger λ in magnitude than that reported here.

The J/ψ polarization is consistent with zero for all transverse momenta but exhibits a 1.8 sigma longitudinal polarization at $p_T > 2$ GeV/c in both the HX and GJ frames when the quadratic sum of the statistical and sys-

TABLE II. J/ψ polarization results in the helicity and Gottfried-Jackson frames. Transverse momentum is in GeV/c. Uncertainties correspond to statistical and systematics, respectively.

p_T	$\langle p_T \rangle$	$\lambda^{HX}_{J/\psi}$	$\lambda^{GJ}_{J/\psi}$
0–1	0.64	$0.15^{+0.12}_{-0.18}{}^{+0.06}_{-0.05}$	$0.61^{+0.39}_{-0.52}{}^{+0.21}_{-0.19}$
1–2	1.47	$-0.10^{+0.09}_{-0.13}{}^{+0.03}_{-0.04}$	$-0.20^{+0.30}_{-0.32}{}^{+0.09}_{-0.10}$
2–5	2.85	$-0.19^{+0.10}_{-0.16} \pm 0.04$	$-0.35^{+0.18}_{-0.22}{}^{+0.06}_{-0.09}$
0–5	1.78	$-0.10^{+0.05}_{-0.09} \pm 0.05$	$-0.16^{+0.18}_{-0.12}{}^{+0.09}_{-0.11}$

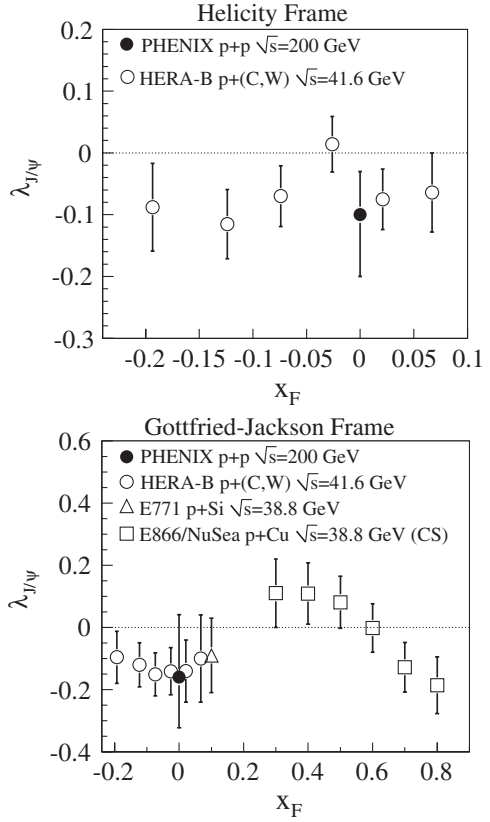

FIG. 9. x_F dependence of J/ψ polarization for $p_T < 5$ GeV/c measured by PHENIX, HERA-B [31], E771 [32], and E866/NuSea (CS frame)[33].

tematic uncertainties are considered. In the HX frame, the p_T dependent λ follows the s-channel cut CSM expectations for prompt J/ψ [41]. Finally, the COM prediction [13], using the nonrelativistic QCD matrix elements fitted to CDF data, is also consistent with our data over the p_T range covered by the calculation.

Figure 9 shows that the polarization for $p_T < 5$ GeV/c follows what is observed in fixed target experiments for a more extended x_F range in the HX and GJ frames. Statistical and systematic uncertainties are quadratically summed for this comparison. Note that the E866/NuSea result was measured in the CS frame.

In principle, intermediate singlet and octet color states may be absorbed differently in the nuclear matter present for fixed target p + A measurements, possibly changing the final J/ψ polarization. The magnitude of nuclear matter effects on J/ψ polarization cannot be resolved with the present data. Direct comparison between future high statistics p_T and rapidity dependence of the J/ψ polarization in $p + p$ and d + Au collisions will provide a better picture for these effects.

V. CONCLUSIONS

We have presented the first J/ψ polarization measurement at RHIC for two different polarization frames. The observed p_T -dependent J/ψ polarization parameter in the HX frame is consistent with the s-channel cut CSM, COM, and no polarization within current uncertainties. The integrated momentum polarization observed in both the HX and GJ frames are in good agreement with the results obtained at fixed target experiments collected in lower energy p + A collision in the same x_F region. Upcoming higher luminosity $p + p$ data will allow more accurate measurements over the full decay angular distributions and over extended p_T and rapidity ranges.

ACKNOWLEDGMENTS

We thank the staff of the Collider-Accelerator and Physics Departments at Brookhaven National Laboratory and the staff of the other PHENIX participating institutions for their vital contributions. We acknowledge support from the Office of Nuclear Physics in the Office of Science of the Department of Energy, the National Science Foundation, a sponsored research grant from Renaissance Technologies LLC, Abilene Christian University Research Council, Research Foundation of SUNY, and the Dean of the College of Arts and Sciences, Vanderbilt University (USA), Ministry of Education, Culture, Sports, Science, and Technology and the Japan Society for the Promotion of Science (Japan), Conselho Nacional de Desenvolvimento Científico e Tecnológico and Fundação de Amparo à Pesquisa do Estado de São Paulo (Brazil), Natural Science Foundation of China (People's Republic of China), Ministry of Education, Youth and Sports (Czech Republic), Centre National de la Recherche Scientifique, Commissariat à l'Énergie Atomique, and Institut National de Physique Nucléaire et de Physique des Particules (France), Ministry of Industry, Science and Tekhnologies, Bundesministerium für Bildung und Forschung, Deutscher Akademischer Austausch Dienst, and A. von Humboldt Stiftung (Germany), Hungarian National Science Fund, OTKA (Hungary), Department of Atomic Energy (India), Israel Science Foundation (Israel), National Research Foundation (Korea), Ministry of Education and Science, Russia Academy of Sciences, Federal Agency of Atomic Energy (Russia), VR and the Wallenberg Foundation (Sweden), the U.S. Civilian Research and Development Foundation for the Independent States of the Former Soviet Union, the US-Hungarian Fulbright Foundation for Educational Exchange, and the US-Israel Binational Science Foundation.

[1] A. Adare *et al.* (PHENIX Collaboration), Phys. Rev. Lett. **98**, 232002 (2007).
[2] C. S. Lam and W.-K. Tung, Phys. Rev. D **18**, 2447 (1978).
[3] K. Gottfried and J. D. Jackson, Nuovo Cimento **33**, 309 (1964).
[4] J. C. Collins and D. E. Soper, Phys. Rev. D **16**, 2219 (1977).
[5] P. Faccioli, C. Lourenco, J. Seixas, and H. K. Wohri, Phys. Rev. Lett. **102**, 151802 (2009).
[6] H. Fritzsch, Phys. Lett. **67B**, 217 (1977).
[7] R. Vogt (private communication).
[8] J. F. Amundson, O. J. P. Eboli, E. M. Gregores, and F. Halzen, Phys. Lett. B **390**, 323 (1997).
[9] R. Baier and R. Ruckl, Phys. Lett. **102B**, 364 (1981).
[10] N. Brambilla *et al.* (Quarkonium Working Group), arXiv: hep-ph/0412158.
[11] J. P. Lansberg, Int. J. Mod. Phys. A **21**, 3857 (2006).
[12] F. Abe *et al.* (CDF Collaboration), Phys. Rev. Lett. **79**, 572 (1997).
[13] H. S. Chung, S. Kim, J. Lee, and C. Yu, Phys. Rev. D **81**, 014020 (2010).
[14] J. M. Campbell, F. Maltoni, and F. Tramontano, Phys. Rev. Lett. **98**, 252002 (2007).
[15] P. Artoisenet, J. P. Lansberg, and F. Maltoni, Phys. Lett. B **653**, 60 (2007).
[16] B. Gong and J.-X. Wang, Phys. Rev. Lett. **100**, 232001 (2008).
[17] P. Artoisenet, J. M. Campbell, J. P. Lansberg, F. Maltoni, and F. Tramontano, Phys. Rev. Lett. **101**, 152001 (2008).
[18] J. P. Lansberg, Eur. Phys. J. C **61**, 693 (2009).
[19] H. Haberzettl and J. P. Lansberg, Phys. Rev. Lett. **100**, 032006 (2008).
[20] G. T. Bodwin, E. Braaten, and G. P. Lepage, Phys. Rev. D **51**, 1125 (1995).
[21] F. Cooper, M. X. Liu, and G. C. Nayak, Phys. Rev. Lett. **93**, 171801 (2004).
[22] M. Beneke and I. Z. Rothstein, Phys. Rev. D **54**, 2005 (1996).
[23] M. Beneke and M. Kramer, Phys. Rev. D **55**, R5269 (1997).
[24] E. Braaten, B. A. Kniehl, and J. Lee, Phys. Rev. D **62**, 094005 (2000).
[25] B. Gong, X. Q. Li, and J.-X. Wang, Phys. Lett. B **673**, 197 (2009).
[26] G. E. Hogan *et al.*, Phys. Rev. Lett. **42**, 948 (1979).
[27] A. R. Clark *et al.*, Phys. Rev. Lett. **45**, 2092 (1980).
[28] C. Biino *et al.*, Phys. Rev. Lett. **58**, 2523 (1987).
[29] A. Gribushin *et al.* (E672 and E706 Collaborations), Phys. Rev. D **53**, 4723 (1996).
[30] C. Akerlof *et al.* (FNAL E537 Collaboration), Phys. Rev. D **48**, 5067 (1993).
[31] I. Abt *et al.* (HERA-B Collaboration), Eur. Phys. J. C **60**, 517 (2009).
[32] T. Alexopoulos *et al.* (E771 Collaboration), Phys. Rev. D **55**, 3927 (1997).
[33] T. H. Chang *et al.* (FNAL E866/NuSea Collaboration), Phys. Rev. Lett. **91**, 211801 (2003).
[34] A. Abulencia *et al.* (CDF Collaboration), Phys. Rev. Lett. **99**, 132001 (2007).
[35] B. L. Ioffe and D. E. Kharzeev, Phys. Rev. C **68**, 061902 (R) (2003).
[36] S. S. Adler *et al.* (PHENIX Collaboration), Nucl. Instrum. Methods Phys. Res., Sect. A **499**, 489 (2003).
[37] GEANT 3.2.1, CERN Computing Library (1993), http://wwwasdoc.web.cern.ch/wwwasdoc/pdfdir/geant.pdf.
[38] A. Adare *et al.* (PHENIX Collaboration), Phys. Rev. C **81**, 034911 (2010).
[39] A. Adare *et al.* (PHENIX Collaboration), Phys. Lett. B **670**, 313 (2009).
[40] P. Faccioli, C. Lourenco, J. Seixas, and H. K. Woehri, J. High Energy Phys. 10 (2008) 004.
[41] J. P. Lansberg and H. Haberzettl, AIP Conf. Proc. **1038**, 83 (2008).